Mech. Sci., 17, 1023–1037, 2026
https://doi.org/10.5194/ms-17-1023-2026
© Author(s) 2026. This work is distributed under
the Creative Commons Attribution 4.0 License.

mechanical sciences

A predictive control strategy of an active heave compensation system for an electric-driven marine winch based on dynamic analysis

Tiancai Xie[1], **Liangpei Huang**[2], **Shaoli Wang**[1], **and Chao Zhong**[1]

[1]School of Mechanical Engineering, Hunan Institute of Engineering, Xiangtan, 411104, China
[2]School of Mechanical Engineering, Hunan University of Science and Technology, Xiangtan, 411201, China

Correspondence: Liangpei Huang (xtcwork@163.com)

Received: 13 May 2026 – Revised: 4 September 2026 – Accepted: 2 October 2026 – Published: 9 November 2026

Abstract. With the influence of wave fluctuation, the engineering ship shows a complex motion with 6 degrees of freedom (6 DOF), which causes a series of problems for offshore operations. Aiming to address this engineering phenomenon, various research projects focusing on dynamics and control have been carried out. However, the relationship between dynamics and control has been severed. This work considers the shortcomings of a simplified model of wire rope and studies the dynamic characteristics of an active heave compensation (AHC) system based on flexible wire rope, as well as the control characteristics of an AHC system based on a marine winch. As a result, an AHC method with model predictive control (MPC) based on dynamic simulation results is proposed, which eliminates the sudden displacement of underwater equipment at the start-up moment of the dynamic, reducing the maximum heave displacement from −0.75 to −0.03 m, while the experiments also prove that the AHC system has the ability to reduce maximum heave displacement from 0.95 to 0.025 m. The overall work is conductive to the research and development of an AHC system and is of practical significance for the exploration of marine resources.

1 Introduction

The marine winch is a significant piece of offshore equipment which is generally used in the hoisting work of underwater equipment (Woodacre et al., 2015). However, under the influence of wave fluctuation, the engineering ship shows a 6-degree-of-freedom (6-DOF) motion, which includes pitch, sway, surge, roll, heave, and yaw. Among them, the heave motion has the most obvious influence on the operations of the marine winch (Xu et al., 2021; Liu et al., 2016). In other words, the operation of the marine winch is seriously disturbed, along with the operation of underwater equipment (Schumacher et al., 2016; Kim et al., 2018). Therefore, some compensation systems are used to decouple the relative motion between the underwater equipment and the engineering ship (Liao et al., 2018; Calnan et al., 2018).

The general process of heave compensation can be seen in Fig. 1; the marine winch is installed on the deck of the engineering ship, making it show a similar motion to the movement of the engineering ship. In general, the wire rope used in the hoisting work can be regarded as a spring-damping system; that is, the heave compensation is accomplished by means of the retraction of the flexible wire rope. When the underwater equipment deviates from its expected location, the marine winch rotates according to the movement of underwater equipment so as to realize the launch and recovery of wire rope. Thus, the underwater equipment is relatively stabilized at its expected location. However, there are many problems in the process of heave compensation that need to be solved, such as dynamic modelling and electrical control.

In this regard, many research projects have been carried out, focusing on two specific aspects in recent years. For instance, regarding the research of dynamic problems, Jin et al. (2021) studied the coupled dynamic response of a tension leg platform under the combined conditions of regular waves, irregular waves, and flows and irregular waves, and the influence of the heading angle on the platform motion was given. However, the tension leg platform is generally a

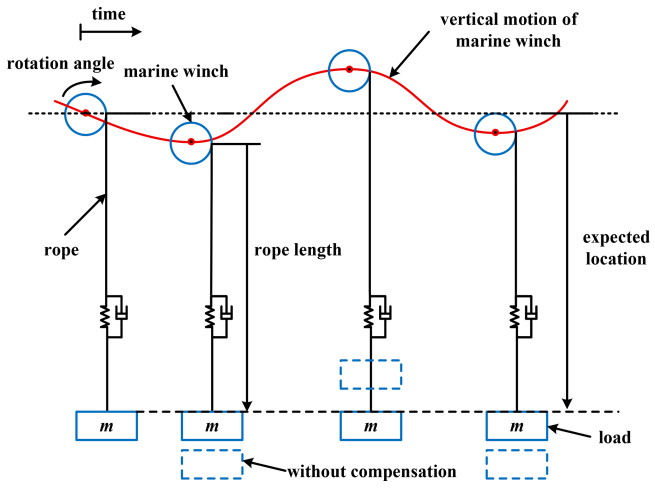


Figure 1. The process of heave compensation.

rigid system; the research can only provide a reference for the dynamic response of the rigid system. Based on the dynamic of a ship-mounted crane, Li et al. (2017) established the mathematical model of the load, and corresponding algorithms have been proposed to suppress the swing of the load. However, the dynamic model used in this work was relatively simple, and the external excitation was also a simplified harmonic excitation. In addition, the influence of heave motion on the system has not been discussed. Che and Wang (2025) considered the coupling relationships among waves, cranes, and loads and analysed the motion characteristics by using the coupling model, revealing the mechanism of load swing. However, this work only used the numerical simulation to verify the assumptions in the work; there were many factors affecting the rationality of the modelling.

Regarding the research on electrical control, the first problem relates to how to study complex waves. For example, Zhang et al. (2017) decomposed the conventional motion of an engineering ship into low-frequency motion and high-frequency motion so as to make a short-term prediction of ship motion under the excitation of regular waves. In particular, the corresponding simulation analyses of turning and tortuous motion were carried out and were also verified by experimental works. However, this work assumed that the regular wave had no effect on the low-frequency hydrodynamic forces acting on the hull, propeller, and rudder, which was in conflict with the actual situation. Lawrence et al. (2018) derived the nonlinear Boussinesq model with optimized dispersion for the applications of wave tank and coastal engineering. Moreover, the comparisons between classical experiments and measured data had previously been carried out, including the comparison of irregular waves in deep water. However, the maritime environment generally involves high-pressure conditions at depths of several kilometres, but the maximum depth in this work did not exceed 2000 m. Based on the analogy of wave buoys, Nielsen et al. (2018) proposed a spectral procedure for estimating the ship motion in a short-crested seaway, while the estimation of the wave spectrum was obtained by means of a direct-brute-force method, and the premise of this approach was based on several assumptions which conflicted with the reality. Secondly, some scholars devoted themselves to the study of control strategy, which can restrain the consequences of 6-DOF motion. Li et al. (2025) used a convolutional neural network algorithm to predict the heave motion of the engineering ship, along with a long-term- and short-term-memory network algorithm. Meanwhile, a high-gain sliding-mode controller was used to compensate for the heave motion of the underwater equipment, while a particle swarm optimization algorithm was used to optimize the parameters of the high-gain sliding-mode controller. Unfortunately, although the complexity of the marine environment had been considered and the irregular waves had been chosen as the external excitation, this work still used the empirical formulas to represent this complex motion. Cuellar et al. (2017) designed a passive heave compensator with the desired frequency response and verified the compensator by means of experiments. However, during the process of offshore drilling, the mass of the spring in the semi-active controller changed severely, which directly affected the performance of the system. Meanwhile, there was excessive noise in the output signal of the controller, and targeted treatment was barely carried out. On the basis of applying an electric-driven hydraulic winch, Huang et al. (2017) proposed a software decoupling control strategy based on the dual closed loop, realizing the stable control of the bottom hole pressure. Similarly, to facilitate the research, this work also simplified the heave motion of the floating drilling platform; the underground working conditions were complex, and the system delay was relatively severe.

Through the above research projects, it can be inferred that it is quite different from reality to simulate complex wave motion by means of empirical formulas and using the method of replacing complex wave motion with simple harmonic motion. In addition, it is obvious that the relationship between dynamic and electrical control is pretty loose, and it is in a split state. Therefore, this work abandons the conventional method of simulating wave motion and directly collects actual wave data in a sea trial by using ship attitude instruments, used as the external excitation of the mechanical system equipped with an active heat compensation (AHC) function. Furthermore, the mathematical model of the flexible wire rope is identified by dynamic results, applied in the simulation of the corresponding control system. Eventually, a control strategy of the AHC system with a model predictive control (MPC) method based on an identified model of the AHC system is proposed, and relevant simulation analyses are carried out. The rest of this paper is organized as follows: Sect. 2 mainly expounds upon the wave types used in this work, and the composition of the heave compensation system is also introduced, which leads to the modelling of the flexible wire rope. After establishing the rigid–flexible coupling

model of the AHC system using ADAMS, the compensation performance of the system and the modelling rationality of the flexible wire rope are verified by simulation results, and the mathematical model of the wire rope is also identified. In Sect. 3, the equation of the multi-axis dragging system based on a marine winch is derived, as well as the equation of a motor speed regulation system based on the MPC method. By combining with the dynamic analysis, the simulation model of the AHC system using the MPC based on the electric-driven marine winch is established, and unambiguous simulation results are obtained. Finally, the conclusion briefly summarizes this work.

2 Modelling and simulation of mechanical system

2.1 Wave description

The wave is a phenomenon that occurs in the ocean and is one of the important forms of movement in seawater. In other words, the wave is the propagation of undulations on the sea surface; it is formed when water particles leave their equilibrium positions and propagate in a certain direction with periodic vibrations, which can be described by Eq. (1) (Zhang et al., 2025).

$$\zeta(t) = \sum_{i=1}^{n} \zeta_{ai} \cos(\omega_{wi} t + \epsilon_i) \tag{1}$$

In the above, $\zeta(t)$ is the original signal, ζ_{ai} denotes the amplitude of the ith harmonic component, ω_{wi} denotes the frequency of the ith harmonic component, and ϵ_i denotes the phase of the ith harmonic component.

According to the variance spectrum of wave displacement, with the frequency of a signal increasing to a negligible extent, the original signal and its spectral density can be expressed by Eq. (2).

$$\begin{cases} \zeta_{ai} = \sqrt{2 S_\zeta \omega_{wi} \Delta\omega_w} \\ S_\zeta(\omega_{wi}) = \frac{8.1\times10^{-3} g^2}{\omega_{wi}^5} \cdot e^{\left(-\frac{3.11}{h_{1/3}^2 \omega_{wi}^4}\right)} \end{cases} \tag{2}$$

In the above, g denotes the acceleration of gravity, and $h_{1/3}^2$ represents the wave height.

However, there is the fact that the simplified formula based on wave energy brings horrible errors into our calculations. Therefore, using data obtained from actual sea trials makes it more reliable (Li et al., 2018). Figures 2 and 3 show the waveform of heave motion measured under level-3 sea conditions and level-4 sea conditions, respectively, so as to reflect the characteristics of external excitation and avoid the adverse effect brought about by empirical formulas as much as possible.

Table 1. Critical indexes of the engineering ship.

Parameter	Value	Unit
Length	130	m
Width	16.4	m
Draught	3.2	m
Displacement	3700	t

2.2 Modelling of the mechanical system

The AHC system equipped with an electric-driven marine winch includes several significant components. As shown in Fig. 4, the marine winch, which is responsible for the recovery and launch of the wire rope, is generally installed in the centre of the deck. Meanwhile, the hoisting sheave is installed on the frame to guide the wire rope. The rotation of the marine winch, however, depends on the corresponding rotation of a three-phase asynchronous motor, which is controlled by the programmable logic controller (PLC). With the above in place, the heave compensation of underwater equipment will be realized. The critical indexes of the engineering ship are shown in Table 1.

With similar characteristics as the hydraulic oil, the wire rope in water can also be regarded to be a spring-damper system to some content (Korde et al., 2016). Meanwhile, there is a certain relationship between the heave displacement of underwater equipment and the vertical motion of the engineering ship, which is revealed by the wire rope (Zhao et al., 2016). Consequently, it is crucial to choose an appropriate modelling method for the wire rope so as to better reflect the relationship between the heave displacement of underwater equipment and the vertical motion of engineering ships, as well as the mechanical characteristics of wire rope. The modelling method of bushing is a method of applying interaction forces to two components, which simulates various properties of the wire rope in a way that is closer to the actual situation (Guo et al., 2018; Huang et al., 2018). In detail, this applies forces and moments to different coordinate systems, realizing the simulation of the nonlinear stiffness and damping characteristics of the wire rope in three-dimensional space. Figure 5 is the stress analysis diagram based on the bushing force.

When applying the bushing force, two coordinate markers are established at the force points of different components. Meanwhile, the calculation of the reaction force and reaction moment will be involved in the calculation of the bushing

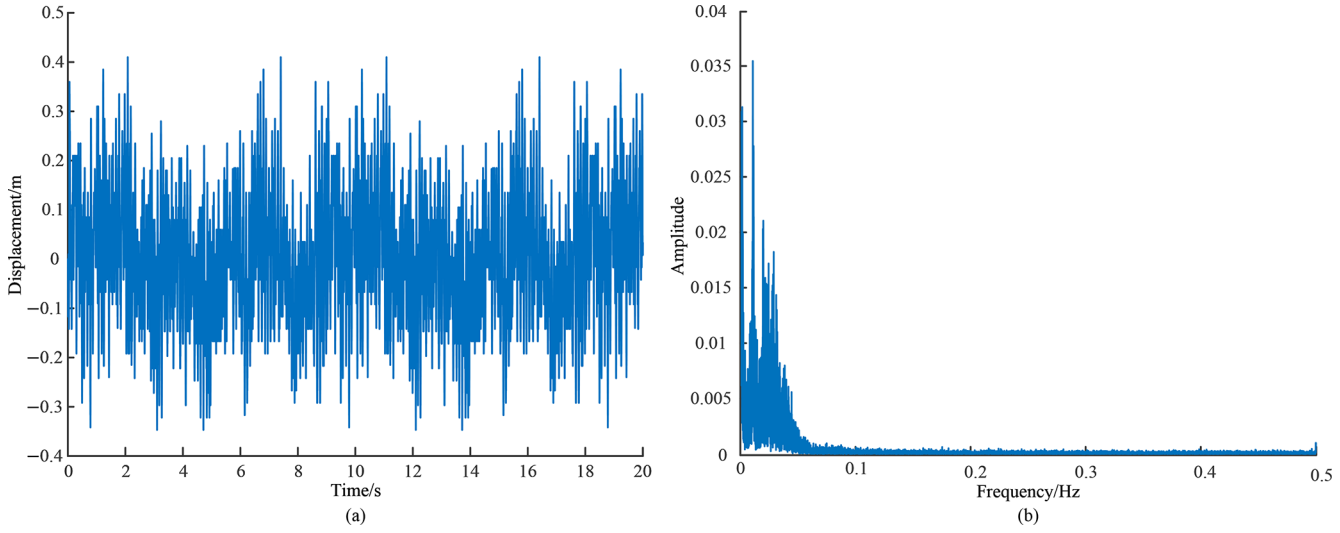


Figure 2. The diagram of level-2 sea condition. **(a)** Time domain diagram; **(b)** frequency domain diagram.

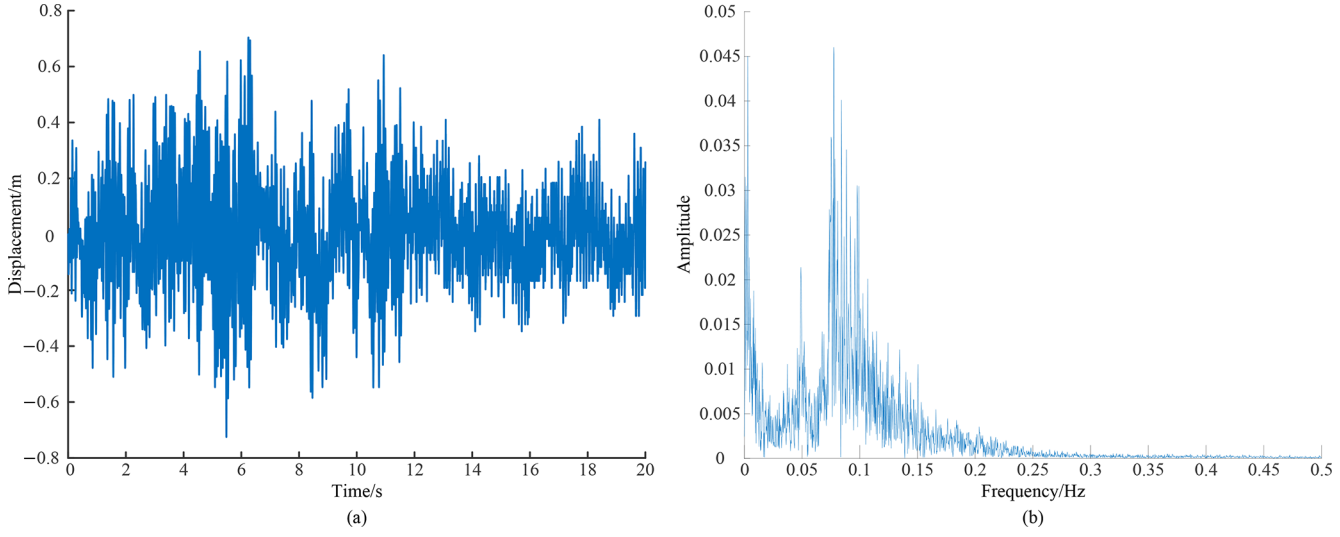


Figure 3. The diagram of level-3 sea condition. **(a)** Time domain diagram; **(b)** frequency domain diagram.

force, which can be seen in Eq. (3).

$$\begin{bmatrix} F_x \\ F_y \\ F_z \\ T_x \\ T_y \\ T_z \end{bmatrix} = \begin{bmatrix} K_{r11} & 0 & 0 & 0 & 0 & 0 \\ 0 & K_{r22} & 0 & 0 & 0 & 0 \\ 0 & 0 & K_{r33} & 0 & 0 & 0 \\ 0 & 0 & 0 & K_{r44} & 0 & 0 \\ 0 & 0 & 0 & 0 & K_{r55} & 0 \\ 0 & 0 & 0 & 0 & 0 & K_{r66} \end{bmatrix} \begin{bmatrix} r_x \\ r_y \\ r_z \\ \theta_x \\ \theta_y \\ \theta_z \end{bmatrix} - \begin{bmatrix} C_{r11} & 0 & 0 & 0 & 0 & 0 \\ 0 & C_{r22} & 0 & 0 & 0 & 0 \\ 0 & 0 & C_{r33} & 0 & 0 & 0 \\ 0 & 0 & 0 & C_{r44} & 0 & 0 \\ 0 & 0 & 0 & 0 & C_{r55} & 0 \\ 0 & 0 & 0 & 0 & 0 & C_{r66} \end{bmatrix} \begin{bmatrix} v_x \\ v_y \\ v_z \\ \omega_x \\ \omega_y \\ \omega_z \end{bmatrix} + \begin{bmatrix} F_{x0} \\ F_{y0} \\ F_{z0} \\ T_{x0} \\ T_{y0} \\ T_{z0} \end{bmatrix} \tag{3}$$

In the above, $\begin{bmatrix} r_x & r_y & r_z & \theta_x & \theta_y & \theta_z \end{bmatrix}^{\mathrm{T}}$ is the matrix of the relative displacement and relative angular displacement, while its coefficient matrix is the stiffness matrix of wire rope. $\begin{bmatrix} v_x & v_y & v_z & \omega_x & \omega_y & \omega_z \end{bmatrix}^{\mathrm{T}}$ represents the matrix of the relative linear velocity and relative angular velocity, while its coefficient matrix is the damping matrix of the wire rope.

There are some relations in the calculation of relevant parameters in the stiffness matrix of the wire rope, shown in Eq. (4).

$$\begin{cases} K_{r11} = EA/L_w \\ K_{r22} = K_{r33} = G_w A/L_w \\ K_{r44} = G_w \pi R^4/2L_w \\ K_{r55} = K_{r66} = E\pi R^4/4L_w \end{cases} \tag{4}$$

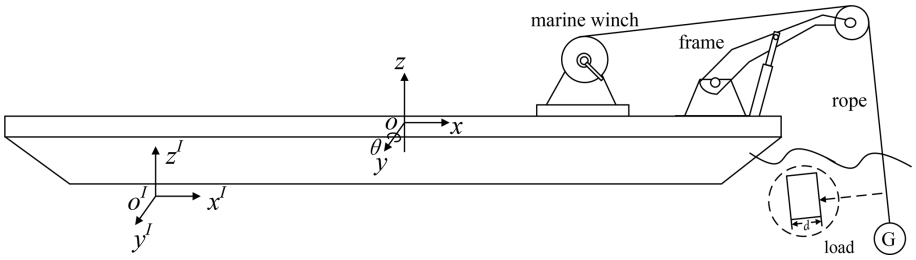


Figure 4. Diagram of the AHC system.

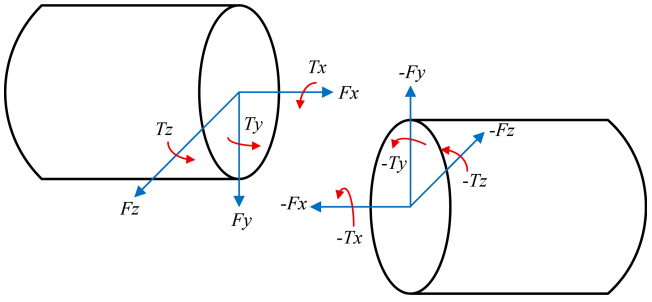


Figure 5. Stress analysis diagram of bushing force.

Table 2. Physical quantities related to stiffness coefficients.

Parameter	Description	Value	Unit
E	Elastic modulus	140 000	$\mathrm{N\,mm^{-2}}$
G_w	Shear modulus	80	GPa
A	Cross-sectional area	804.25	$\mathrm{mm^2}$
R	Radius	16	mm
L_w	Length of micro-segment	100	mm

In the above, K_{r11} denotes the coefficient of tensile stiffness, K_{r22} and K_{r33} denote the coefficients of shear stiffness, K_{r44} denotes the coefficient of torsional stiffness, and K_{r55} and K_{r66} denote the coefficients of bending stiffness. Meanwhile, other physical quantities related to the calculation of relevant stiffness coefficients are listed in Table 2.

During the process of AHC, there will be collision and friction between the wire rope and rope-crossing device. Therefore, it is necessary to take the mechanical properties of different components into consideration. The contact can describe the mechanical phenomenon accurately, often characterized by an impulse function method (Ma et al., 2021). The definition of the impulse function is described using Eq. (5).

$$F_c = \begin{cases} 0 & x_c > 0 \\ K_c x_c^e + \mathrm{STEP}(x_c, 0, 0, x_{c_{\max}}, c_{\max})\dot{x}_c & x_c \le 0 \end{cases} \quad (5)$$

In the above, K_c is the coefficient of the contact surface, x_c is the depth of contact, $x_{c_{\max}}$ is the maximum depth of contact, $c_{\max}$ is the maximum damping coefficient of contact, e is the nonlinear collision coefficient of contact, and STEP represents the step function.

In general, the coefficient of the contact surface is affected by the difference in geometry and structure between two objects. At present, however, there is no accurate formula that can be used to calculate it, and it is mainly calculated according to the empirical formula, which is shown in Eq. (6).

$$\begin{cases} K_c = \frac{4}{3} R_c^{\frac{1}{2}} E^* \\ \frac{1}{R_c} = \frac{1}{R_1} + \frac{1}{R_2} \\ \frac{1}{E^*} = \frac{1-\delta_1^2}{E_1} + \frac{1-\delta_2^2}{E_2} \end{cases} \quad (6)$$

In the above, R_1 and R_2 represent the effective radius, E_1 and E_2 represent Young's modulus, and δ_1 and δ_2 represent Poisson's ratio.

As mentioned earlier, the external excitation used in the simulation involved in this work is the actual data collected by the inertial measurement unit (IMU) under level-3 sea conditions and level-4 sea conditions, while the diagrams of filtered data imported by the SPLINE interpolating method are shown in Fig. 6. According to the principle of heave compensation, the corresponding rotation can be applied to the drum on the premise of knowing the variation rules of the engineering ship's heave motion. In this way, the influence of the engineering ship's movement on the offshore operation can be weakened to a certain extent.

2.3 Simulation of the mechanical system

As can be seen in Fig. 7, the AHC system involved in this work is mainly composed of six asynchronous motors, an electric-driven marine winch, a frame, and wire rope. Due to the fact that the heave motion has the greatest influence on the offshore operation with 6-DOF motion, this work focuses on the compensation of heave motion. In addition, the flexibility of wire rope is increased by using the bushing-force modelling method, while the accuracy of the modelling method can be verified by the mechanical characteristics of the wire rope, as well as the normal function of AHC.

As can be seen in Fig. 8, the engineering ship shows a similar heave motion as wave fluctuation under the excitation of measured waves, and there is only a slight difference in amplitude between them. In detail, the displacement of equipment varies between -0.8 to $+0.6$ m under the traction of the wire rope, while the displacement of equipment is greatly

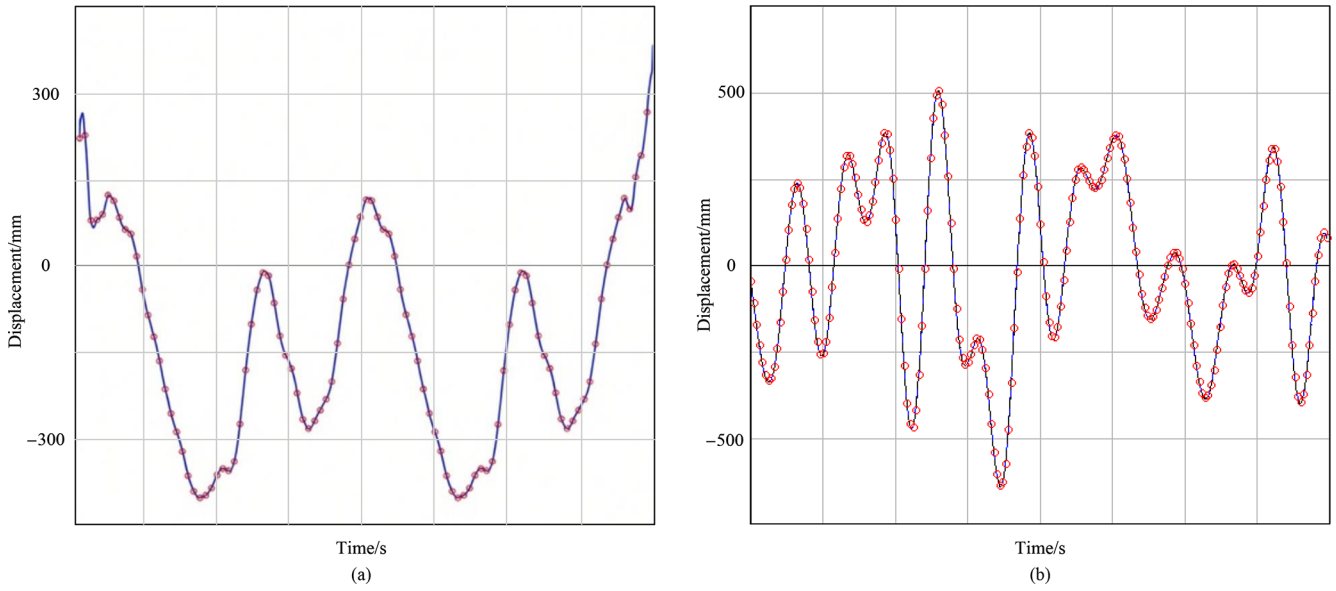


Figure 6. Filtered data of different sea conditions. **(a)** Level-2 sea condition; **(b)** level-3 sea condition.

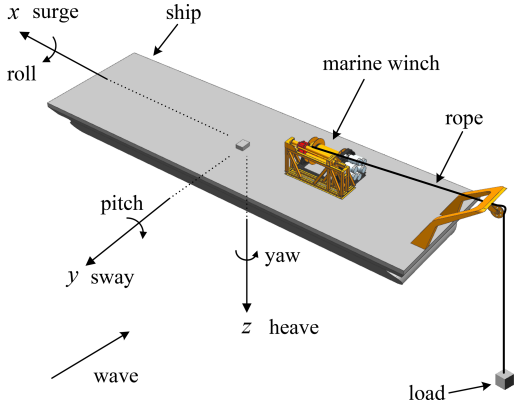


Figure 7. Dynamic simulation model of the AHC system.

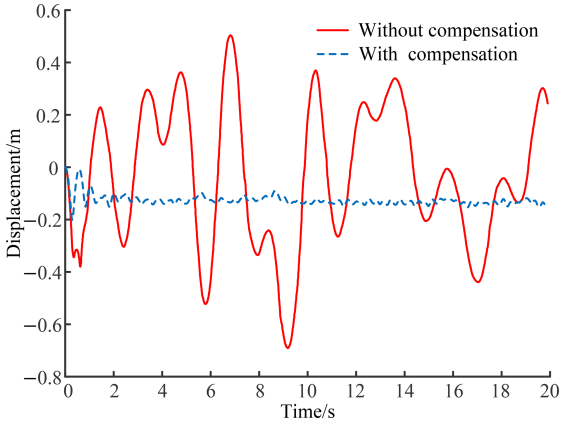


Figure 8. Variation in equipment displacement.

reduced after the AHC function is enabled. However, at the initial stage of AHC, the displacement of equipment indicates that the compensation function needs to be optimized, and the equipment is not completely stable at its expected position.

To verify the system performance under different loads, the corresponding simulations have been carried out, while the load displacements and rope tensions under different loads are shown in Fig. 9. On the one hand, when the underwater equipment is placed at a certain depth, the average load displacement is about −0.05 m when the load is 25 kN, and the average load displacement is about −0.13 m when the load is 55 kN, while the average load displacement is about −0.17 m when the load is 85 kN. In other words, the heavier the underwater equipment, the more it deviates from the ideal position. Meanwhile, the frequency of its displacement decreases accordingly. On the other hand, the tension of the wire rope ranges from 0 to 140 kN when the load is 25 kN, and the tension of the wire rope ranges from 0 to 275 kN when the load is 55 kN, while the tension of the wire rope ranges from 0 to 290 kN when the load is 85 kN. It is clear that, as the underwater equipment becomes heavier, the tension of the wire rope also increases.

As shown in Fig. 10, when the load is made up of a specific piece of marine equipment, the average load displacement is about −0.13 m when the depth is 1000 m, and the average load displacement is about −0.15 m when the depth is 2000 m, while the average load displacement is about −0.18 m when the depth is 3000 m. It is obvious that the deeper the load locates, the greater its average heave displacement is. In addition, the tensions of the wire rope range

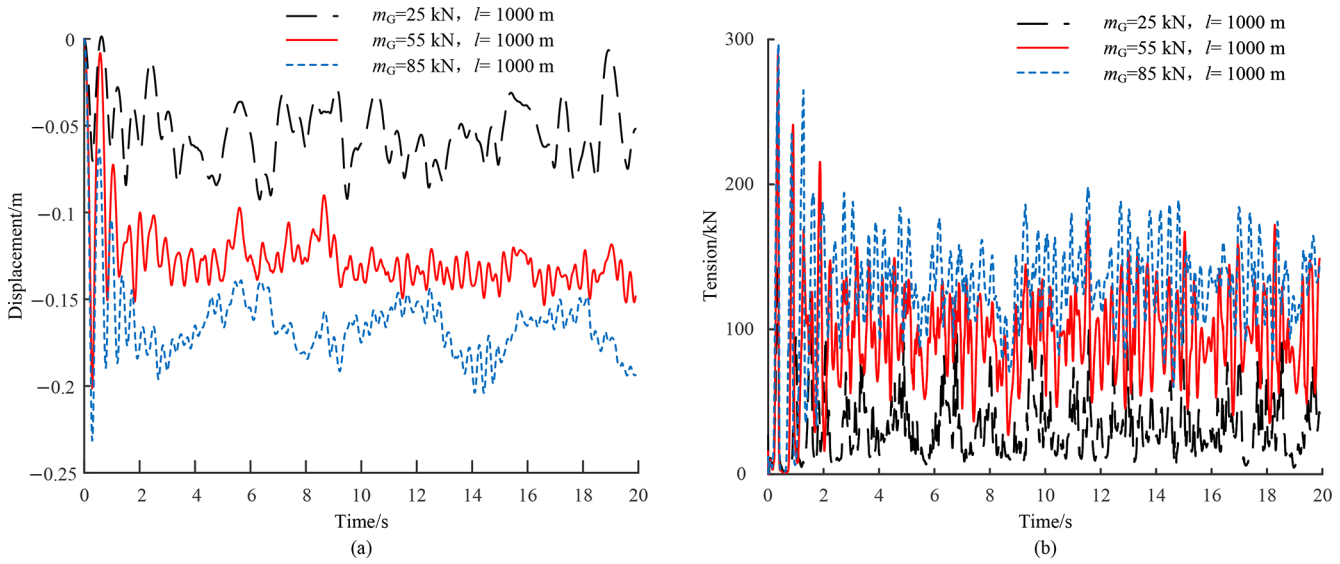


Figure 9. The dynamic simulation results of the AHC system under different loads. **(a)** Load displacements under different loads; **(b)** rope tensions under different loads.

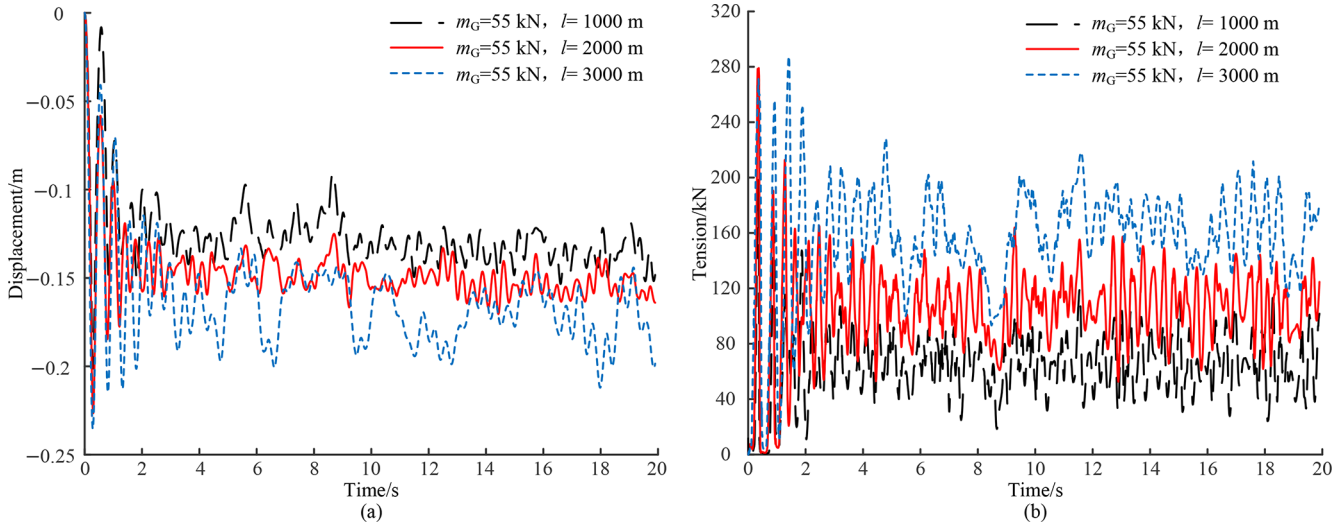


Figure 10. The dynamic simulation results of the AHC system at different depths. **(a)** Load displacements at different depths; **(b)** rope tension at different depths.

from 0 to 275, 0 to 280, and 0 to 290 kN, respectively, under the above three conditions.

From the average values of the simulation results under different conditions, it can be inferred that the static characteristics of wire rope are well simulated. Meanwhile, by observing the curves of the simulation results, the dynamic characteristic of flexible wire rope has also been well simulated, which proves that the modelling method of flexible wire rope is reasonable.

2.4 Identification of mechanical system

Most research projects generally take the long wire rope used for marine operations as a spring damper system, which causes the relationship between load displacement and ship displacement and between load displacement and drum angle to be inaccurate. However, the system identification method makes the clarification of the mathematical model a reality (Zhou et al., 2024). In addition, the system identification involved in this work mainly focuses on the relationships among load displacement, ship displacement, and drum angle directly.

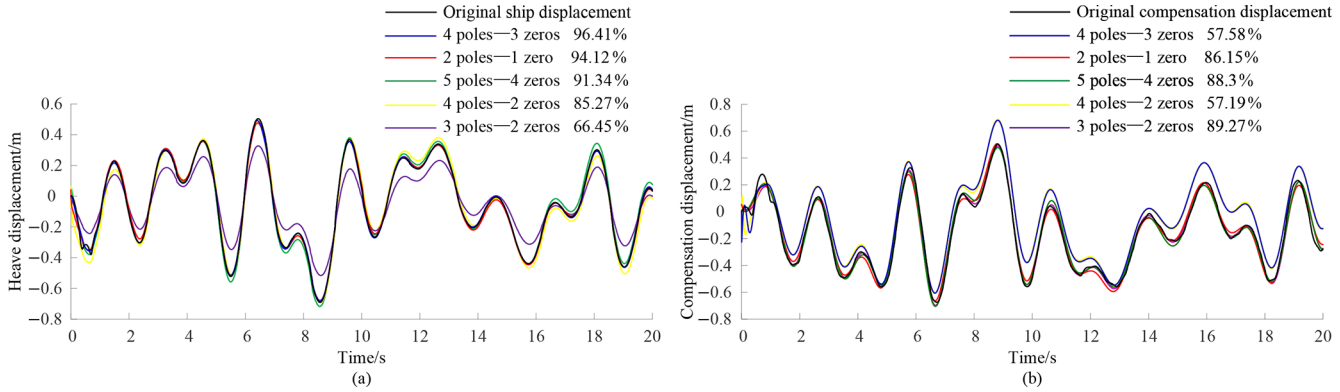


Figure 11. Identification results based on dynamic analysis. **(a)** Load displacement to ship displacement; **(b)** load displacement to drum angle.

The identification results based on dynamic analysis are shown in Fig. 11. Apparently, the system identification is carried out through different poles and zeros. In detail, from the identification results of load displacement to ship displacement, when the transfer function is selected as the structure of four poles and three zeros, the percentage of the identification result is 96.41 %, while the percentage of the identification result is 66.45 % when the transfer function is selected as the structure of three poles and two zeros. In addition, from the identification result of the transfer function for load displacement to drum angle, the percentage of the best identification result is 89.27 %, and the worst is 57.19 %. The detailed identification results of transfer functions are shown in Table 3.

3 Modelling and simulation of control system

3.1 Modelling of control system

The structure of a multi-motor driving system can greatly enhance the reliability of a work, and the structure of six motors is selected in this work. The motion equation of a multi-motor driving system is shown in Eq. (7).

$$6T_{\mathrm{e}} - T_{\mathrm{L}} = \frac{\mathrm{GD}^2}{375}\frac{\mathrm{d}n}{\mathrm{d}t} \tag{7}$$

In the above, T_{e} is the output torque of the motor, T_{L} is the resisting torque of the load, n is the motor speed, and GD^2 is the flywheel torque.

The resisting torque of the load is shown in Eq. (8).

$$T_{\mathrm{L}} = \frac{\left(G_0 + mr\frac{\mathrm{d}^2\theta}{\mathrm{d}t^2}\right)r}{i} \tag{8}$$

In the above, m is the equivalent load mass, G_0 is the static load, r is the radius of the drum, θ is the drum angle, and i is the total transmission ratio of system.

According to the principle of the Laplace transform method, the relationship between drug angle and motor torque can be represented by the transfer function, which is written as Eq. (9).

$$\frac{\theta(s)}{T_{\mathrm{e}}(s)} = \frac{6}{\left(\frac{2\mathrm{GD}^2}{25\pi} + \frac{mr^2}{i}\right)s^2} \tag{9}$$

With electromagnetic interference, opening and closing of the relay, the rotational inertia of drum, and the mechanical characteristics of flexible wire rope, which exist objectively, there is an inevitable time delay in the control system of the electric-driven marine winch. Therefore, the AHC action is always inconsistent with the motion of underwater equipment, making it necessary to carry out the research on AHC with MPC, which can effectively solve the time delay caused by many factors (Tischler, 2018; Richter et al., 2017).

In general, the drum is driven by a three-phase asynchronous motor through the transmission mechanism, while the voltage equation of the rotor flux oriented vector control system can be expressed as Eq. (10).

$$\begin{cases} u_{sd} = R_{\mathrm{s}}i_{sd} + \sigma L_{\mathrm{s}}si_{sd} - \omega_{\mathrm{s}}\sigma L_{\mathrm{s}}i_{sq} + \frac{L_{\mathrm{m}}}{L_{\mathrm{r}}}\frac{\mathrm{d}\psi_{\mathrm{r}}}{\mathrm{d}t} \\ u_{sq} = R_{\mathrm{s}}i_{sq} + \sigma L_{\mathrm{s}}si_{sq} + \omega_{\mathrm{s}}\sigma L_{\mathrm{s}}i_{sd} + \frac{L_{\mathrm{m}}}{L_{\mathrm{r}}}\omega_{\mathrm{s}}\psi_{\mathrm{r}} \end{cases} \tag{10}$$

In the above, u_{sd} and u_{sq} denote the stator voltage along the d–q axis, i_{sd} and i_{sq} denote the stator current along the d–q axis, R_{s} denotes the stator resistance, σ denotes the leakage inductance coefficient, L_{s} denotes the stator inductance, L_{r} denotes the rotor inductance, L_{m} denotes the mutual induction of the motor, ω_{s} denotes the angular frequency of the stator, ψ_{r} denotes the rotor flux linkage, and s denotes the differential term.

The voltage equation under steady-state conditions can be further written as Eq. (11).

$$\begin{cases} u_{sd} = R_{\mathrm{s}}i_{sd} - \omega_{\mathrm{s}}\sigma L_{\mathrm{s}}i_{sq} \\ u_{sq} = R_{\mathrm{s}}i_{sq} + \omega_{\mathrm{s}}\sigma L_{\mathrm{s}}i_{sd} \end{cases} \tag{11}$$

Moreover, the electromagnetic torque equation of an asynchronous motor under steady-state conditions can be ex-

Table 3. Detailed identification results of transfer functions.

Type	Transfer function of load displacement to ship displacement	Transfer function of load displacement to drum angle
Two poles–one zero	$\frac{100.6s-5.338}{s^2+98.95s+0.000001372}$	$\frac{-0.08221s-0.003266}{s^2+5.155s+0.001134}$
Three poles–two zeros	$\frac{978.8s^2+317.1s+11.57}{s^3+1420s^2+210.8s+7.479}$	$\frac{-0.0148s^2-0.7909s-0.02843}{s^3+10.38s^2+54.1s+0.0004976}$
Four poles–two zeros	$\frac{4477s^2+337.3s+13.23}{s^4+21.59s^3+4370s^2+729.7s+17.64}$	$\frac{2746s^2-28\,110s-41\,710}{s^4+1632s^3+115\,900s^2+2\,507\,000s+1\,946\,000}$
Four poles–three zeros	$\frac{50.36s^3+137.2s^2+120s-3.645}{s^4+48.17s^3+144.1s^2+117.2s+0.003758}$	$\frac{-281.1s^3+2317s^2-29\,540s-41\,900}{s^4+11890s^3+115\,800s^2+2\,507\,000s+1\,946\,000}$
Five poles–four zeros	$\frac{374.8s^4+1355s^3+1007s^2+425.3s-1.009}{s^5+358.9s^4+1300s^3+1008s^2+452s+15.36}$	$\frac{-0.05997s^4-0.2498s^3-0.2166s^2-0.1179s-0.007106}{s^5+6.486s^4+19.72s^3+14.84s^2+6.966s+5\,115\,000}$

pressed as Eq. (12).

$$T_e = \frac{3}{2} n_p \frac{L_m^2}{L_r} i_{sd} i_{sq} \tag{12}$$

In the above, n_p denotes the pole pairs of the motor.

By substituting Eq. (11) into Eq. (12) and assuming that the stator voltage is ignored, the torque equation under steady-state conditions, expressed by voltage, can be written as Eq. (13).

$$T_e = -\frac{3}{2} \frac{n_p L_m^2}{L_r L_s^2 \sigma} \frac{u_{sd} u_{sq}}{\omega_s^2} \tag{13}$$

Meanwhile, the multi-dimensional prediction should be avoided in the process of MPC, and there should also be a more accurate relationship between drum angle, electromagnetic torque, and input voltage. Therefore, the voltage equation expressed in Eq. (10) should be regarded as the combination of two one-dimensional equations, which can be written as Eq. (14).

$$\begin{cases} \frac{\mathrm{d}i_{sd}}{\mathrm{d}t} = -\frac{R_s}{\sigma L_s} i_{sd} + \frac{u_{sd}}{\sigma L_s} \\ \frac{\mathrm{d}i_{sq}}{\mathrm{d}t} = -\frac{R_s}{\sigma L_s} i_{sq} + \frac{u_{sq}}{\sigma L_s} \end{cases} \tag{14}$$

According to the principle of MPC, the mathematical expression based on the discrete model of the motor can be written as Eq. (15).

$$x_m(k+1) = \mathbf{A}_m x_m(k) + \mathbf{B}_m u(k) \tag{15}$$

In the above, $x_m(k+1)$ denotes the present state variable of the vector control system, $x_m(k)$ denotes the previous state variable of the vector control system, $u(k)$ denotes the control variable of the system, and $\mathbf{A}_m$ and $\mathbf{B}_m$ denote the dynamic matrixes of the system.

By imitating the expression of MPC and applying the Euler discretization method to Eq. (14), the discrete predictive model can be obtained as Eq. (16), where the stator current is regarded as the state variable and the stator voltage is regarded as the control variable.

$$\begin{aligned} i_{sd-q}(k+1) &= i_{sd-q}(k) + \left(-\frac{R_s}{\sigma L_s} i_{sd-q}(k) + \frac{u_{sd-q}(k)}{\sigma L_s} \right) T_s \\ &= \left(1 - \frac{R_s T_s}{\sigma L_s} \right) i_{sd-q}(k) + \frac{T_s}{\sigma L_s} u_{sd-q}(k) \\ &= \mathbf{A}_m i_{sd-q}(k) + \mathbf{B}_m u_{sd-q}(k) \end{aligned} \tag{16}$$

Furthermore, the control variable can be expressed as Eq. (17).

$$u_{sd-q}(k) = \frac{\sigma L_s}{T_s} \left[i_{sd-q}(k+1) - \left(1 - \frac{R_s}{\sigma L_s} T_s \right) i_{sd-q}(k) \right] \tag{17}$$

In the above, $u_{sd-q}(k)$ denotes the control variable of the system, and $i_{sd-q}(k+1)$ denotes the present state variable of the current loop along the d–q axis.

In fact, there are many factors such as system parameters and electrical interference which always leads to a certain deviation between the predicted value and the theoretical value of the controlled object. Thus, it is necessary to optimize the control variable by using feedback correction. The form of the cost function as shown in Eq. (18) can be adopted.

$$\begin{aligned} \min j(k) = &\sum_{i=1}^{p_c} q_i [x_t(k+i) - x_m(k+i)]^2 \\ &+ \sum_{j=1}^{m_c} r_j \Delta u(k+j-1)^2 \end{aligned} \tag{18}$$

In the above, $x_t(k+i)$ denotes the theoretical output value at the moment of $k+i$, $x_m(k+i)$ denotes the actual output value at the moment of $k+i$, $\Delta u(k+j-1)$ denotes the anti-interference function, p_c denotes the optimal period, m_c denotes the control period, and q_i and r_j denote the corresponding weighting coefficients.

It is clear that the optimization problem is transformed into the solution of Eq. (18). That is to say, the rolling optimal model of the control variable is the solution of $\mathrm{d}j(k)/\mathrm{d}\Delta u(k) = 0$.

The structure of the speed regulation system with MPC is shown in Fig. 12. This work uses the MPC method

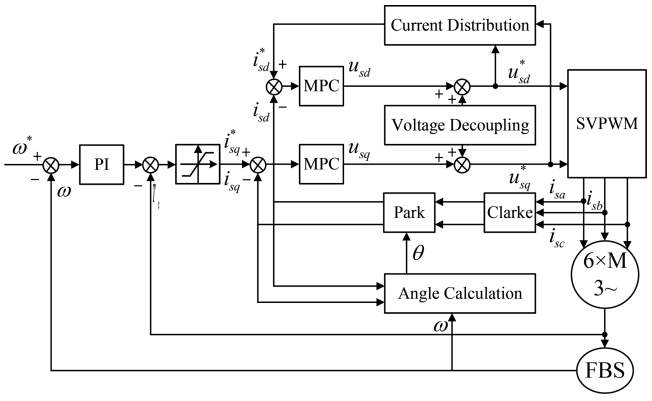


Figure 12. Diagram of the speed regulation system with MPC.

to replace the proportion integration differentiation (PID) method to adjust the current in the circuit so as to improve the ability of the AHC function. In detail, the six motors are controlled by three frequency converters in total, while a primary–secondary synchronization scheme is employed, with the main motor using a speed closed-loop control and the primary motors adopting the following control method via torque.

3.2 Simulation of the control system

In general, the AHC system can be divided into velocity compensation and position compensation (Woodacre et al., 2018). The method of position compensation can not only meet the performance requirement of rapid response but also effectively suppress external interference. However, if there is a requirement that the underwater equipment return to equilibrium at a high speed then enough torque of the system should be ensured. It can be inferred from Fig. 8 that the load displacement after compensation is not located at the expected position. Meanwhile, the compensation has a certain time delay, which shows a large displacement at the initial stage of compensation. To solve this problem, this work uses the method of position compensation with MPC to realize the heave compensation of underwater equipment.

As shown in Fig. 13, the simulation model of the AHC system with the MPC method has been built. In detail, the module named "YY_Adams" denotes the port for importing measured wave data, and the load displacement under wave excitation can be obtained when the wave data pass through the transfer function named "ship displacement–load displacement". Meanwhile, the compensated-for load displacement can be obtained when the output torque of the motor passes through the transfer functions named "motor torque–drum angle" and "drum angle–load displacement" in turn, realizing the AHC function based on the MPC method.

Figure 11 shows the identification results of the load displacement to the drum angle, while identification percentages of four poles–two zeros and four poles–three zeros are less than 60 %, which might have serious effects on the compensation accuracy. As shown in Fig. 14, the compensation effect of the AHC system under different conditions has been emphasized. It is obvious that the compensation effect of the AHC system in the first two cases is still not ideal even if the MPC method is adopted. At worst, the compensation of the AHC system is out of control. In addition, the average identification percentages are over 85 % in the remaining cases. By comparing with the displacement of underwater equipment with poor structures, the compensated-for displacement of underwater equipment in the remaining cases is reduced by an order of magnitude. As shown in Fig. 14c, the load displacement of five poles–four zeros is slightly larger than the load displacement of three poles–two zeros, while the load displacement of three poles–two zeros is obviously larger than the load displacement of two poles–one zero. Anyway, the result shows that the compensation performance of the system has been greatly improved.

As shown in Fig. 15, the effect of the AHC system with two kinds of control strategies under different sea conditions can be observed. Apparently, the harsh sea condition leads to more intense movement of underwater equipment, while the equipment tends to move near the expected position after the heave compensation function with different control strategies is applied. Moreover, by comparing with the compensation effect of the AHC system shown in Fig. 8, the two methods not only reduce the load displacement further but also eliminate the large displacement at the initial stage of compensation, which is of more benefit to the marine operation.

To explore the compensation performance of the system under different loads, this work carried out the relevant simulations, and the results are shown in Fig. 16. Compared with Fig. 15, it can be seen that, when the load increases, the frequency of the load movement slows down obviously. Meanwhile, the variation range of the load displacement expands accordingly. After being compensated for by the sliding-mode controller (SMC), the maximum heave displacement of the load is close to 0.1 m and is even worse when the sea condition gets worse. However, the load displacement compensated for by the MPC controller is significantly reduced, which shows that the working position of the load under this control strategy is more stable and more suitable to the requirements of marine operations.

The simulation results at different depths are shown in Fig. 17; it can be inferred that the movement of the load and the movement of the engineering ship are out of synchronization when the working position of the load gets closer to the seabed. Meanwhile, the range of load movement shows a sign of expanding more than before. In addition, the mentioned control strategies can still achieve a reasonably good compensation effect, while the effect of the MPC controller is also better than that of the SMC controller.

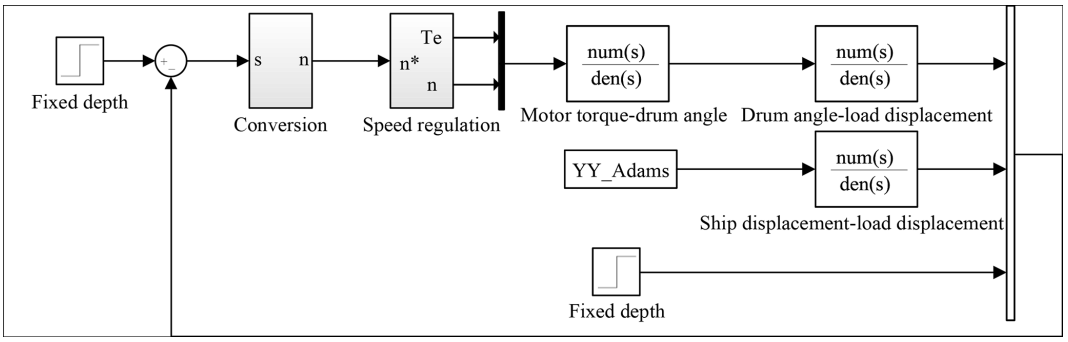


Figure 13. Simulation model of the AHC system with MPC.

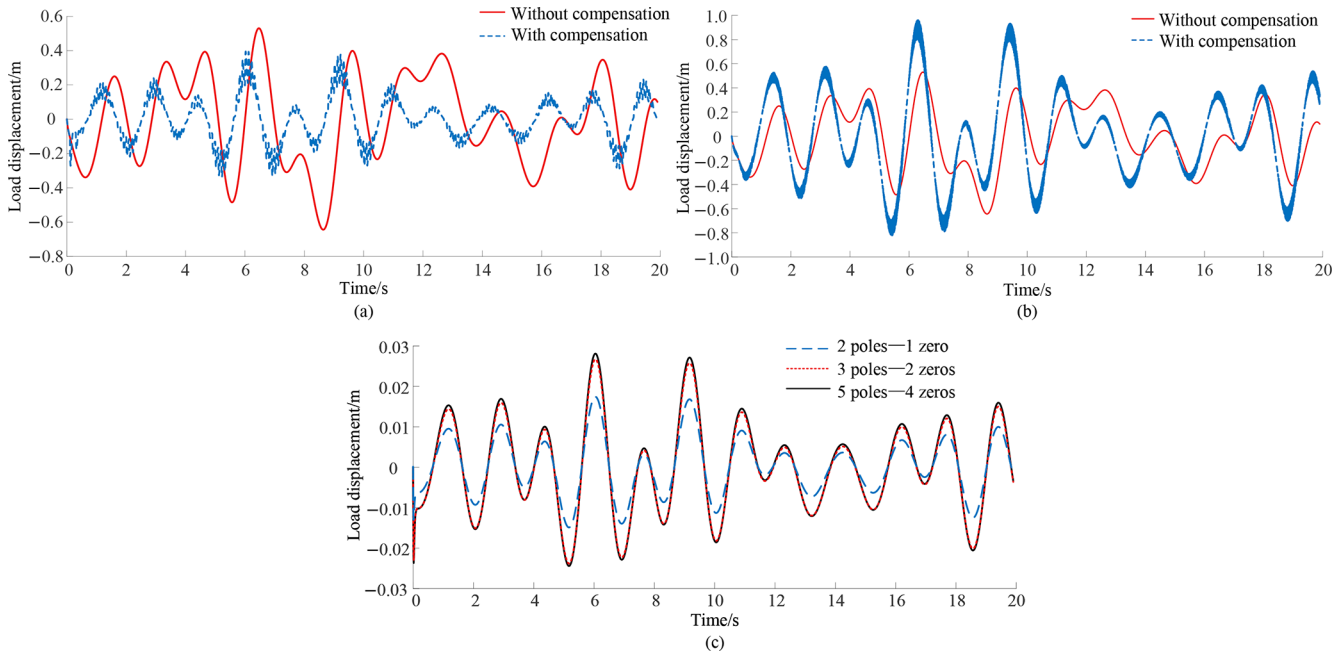


Figure 14. Compensation effect of AHC system with different poles and zeros. **(a)** Four poles and two zeros, **(b)** four poles and three zeros, **(c)** suitable poles and zeros.

4 Experiments

To verify the correction of the simulations, the indoor pool experiment was carried out on the test platform based on the JH-20/45 electric-driven marine winch. As shown in Fig. 18, the test platform is composed of a marine winch, steel wire rope, a mass block, and a remote control terminal, while the mass block is connected with the marine winch through a crown block system. The AHC function is applied to the marine winch by programming through PLC, and the test data collected by the encoder are converted into the heave displacement, which is displayed on the monitoring interface of the remote control terminal. Meanwhile, the water in the pool is not static, and the process of drainage and water supply is dynamic, which makes the situation closer to the current. Moreover, the indoor pool is equipped with a set of wind turbines so as to simulate the sea breeze more realistically. However, this work mainly focuses on the research of heave motion, which means the 6-DOF motion is not fully reflected. In addition, although the overall configuration of the indoor pool could reflect the nonlinear hydrodynamic effect to a certain extent, this degree is not sufficient.

The proposed experimental scheme supposes that the marine winch is fixed on the ground, while the measured data under level-3 sea conditions are imported as the external excitation of AHC system. When all of the preparations are completed, the AHC test with loads of 55 and 115 kN is repeated three times, and the average values of different experiments are used as the critical parameters to evaluate the system performance. It can be seen from Fig. 19 that the maximum load displacement is reduced from 0.95 to 0.025 m when the load is 55 kN, while the maximum load displace-

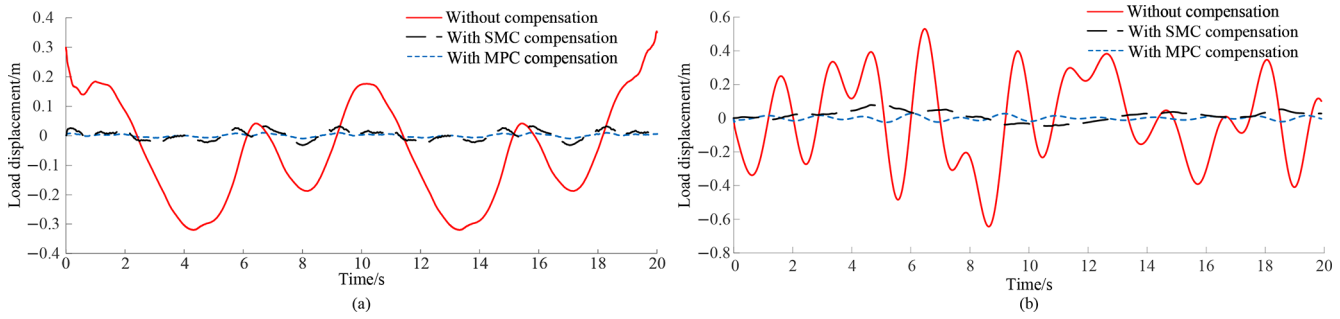


Figure 15. Compensation effect of the AHC system under different sea conditions. **(a)** Level-2 sea condition, **(b)** level-3 sea condition.

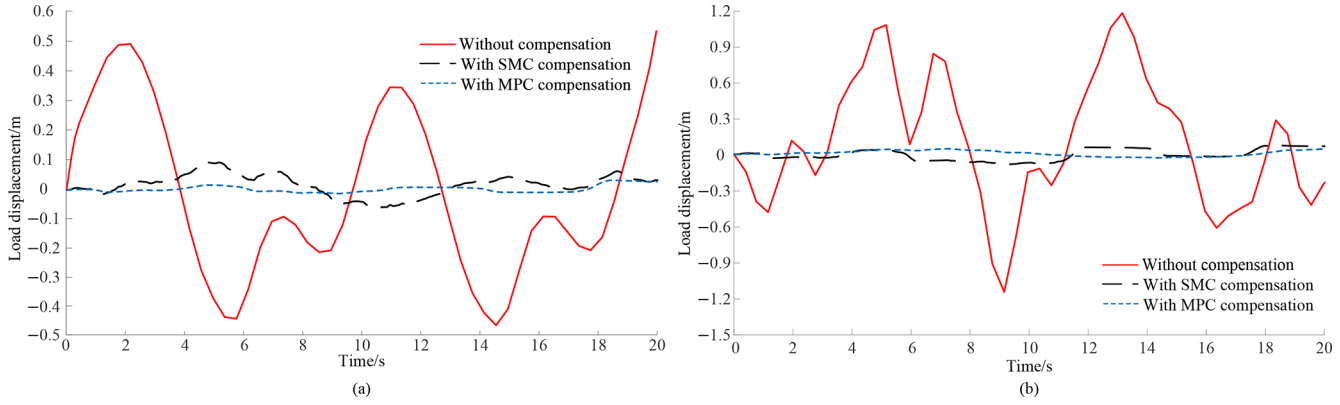


Figure 16. Compensation effect of the AHC system with different loads. **(a)** Level-2 sea condition, **(b)** level-3 sea condition.

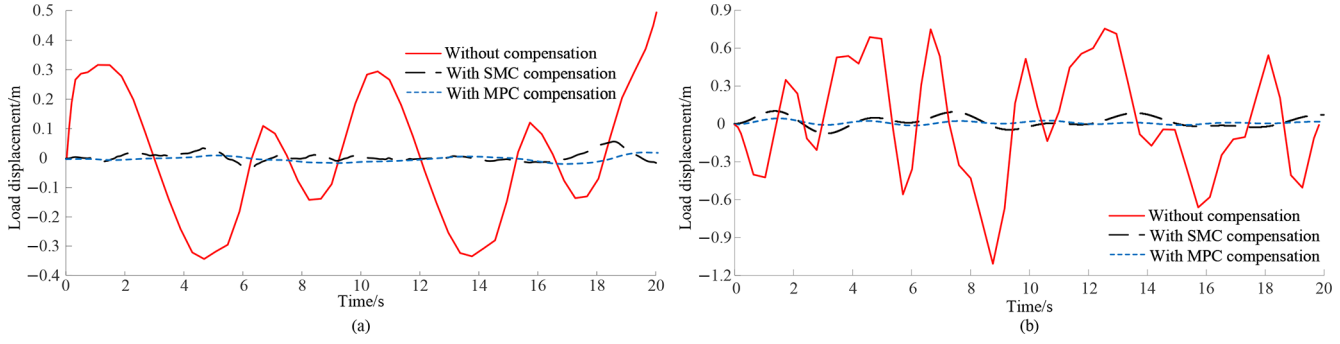


Figure 17. Compensation effect of the AHC system at different depths. **(a)** Level-2 sea condition, **(b)** level-3 sea condition.

ment is reduced from 1.17 to 0.06 m when the load is 115 kN, which proves that the compensation performance of AHC system is ideal enough.

Compared with previous research projects, the modelling process of the virtual prototype is relatively rigorous, not only considering the modelling rationality of overall system but also fully taking into consideration the modelling details such as rope groove and material. From the final control effect, previous research projects also achieved a good control effect, but the research methods still need to be optimized. For example, based on the hydraulic winch, Li et al. (2018) used a nonlinear robust controller to reduce the maximum heave displacement of the load from 1.4 to 0.01 m, while the fluctuation range of rope tension was reduced from 15 kN to less than 1 kN. However, the concrete model of the wire rope was ignored, and only the state space equation of the system was used. Similarly, Xu et al. (2021) used the sliding-mode method to keep the tracking error of the hydraulic winch between −0.03 to +0.03 m; the mechanical properties of the wire rope were also not to be considered. Furthermore, Liao et al. (2018) used active a disturbance rejection method instead of the PID method to improve the compensation accuracy of the marine winch from 0.06 to 0.04 m, and the adjustment time was shortened by



Figure 18. Experimental platform for the AHC system.

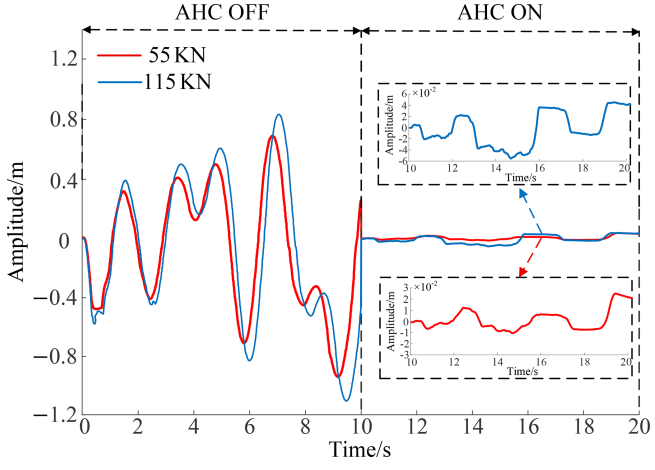


Figure 19. Experimental results under different loads.

5 s. The deficiency of this work is the simplification of the external excitation, while the calculations of the load motion and rope tension were deduced by empirical formulas, which is idealistic. Richter integrated the heave motion prediction algorithm and trajectory-planning algorithm, realizing an appropriate compensation effect when the prediction interval was short. However, it can be seen that load displacement was calculated through the relationship between the drum radius and angular velocity without considering the mechanical properties of the wire rope. Meanwhile, the excitation used in this work was based on empirical formulas cited from previous research. It is obvious that this work overcomes the shortcomings of previous works, such as the simplification of complicated waves, oversight of the mechanical characteristics of the wire rope, and rough modelling of the virtual prototype and the control strategies needed to be optimized, while the experiment results also prove that the method proposed in this work is feasible. Last but not the least, the path towards full-scale offshore implementation and validation is to carry out the scenario-based tests under actual marine conditions by utilizing the national marine test facilities. As far as this work is concerned, further efforts could consider the creation and testing of an experimental platform on a reduced scale.

5 Conclusions

This work mainly focuses on the intelligent control method of the electric-driven marine winch. To achieve this, this work integrates a dynamic analysis method and an MPC method. In detail, on the one hand, by establishing the virtual prototype model of the system with a flexible wire rope, the rationality of system modelling and the AHC function have been preliminarily verified. The simulation results show that the heave displacement of underwater equipment is reduced from −0.73–+0.51 to −0.2–0 m, while the compen-

sation rate is approximately 77 %. In addition, the specific relationship between ship motion and load motion has been explored, along with the relationship between load motion and drum angle. On the other hand, this work takes position compensation based on MPC as the compensation method, and the large displacement at the initial stage of compensation in the dynamic method has been eliminated, which greatly improves the precision of heave compensation, with the compensation rate having increased from 77 % to 96 %. In addition, corresponding experiments have also been carried out to verify the simulation results, and the compensation rates under different loads are 97.4 % and 94.9 %.

However, this work is carried out under level-2 and level-3 sea conditions collected in the specific sea trial, causing the AHC function to be aimed at these specific excitations, while the AHC functions under other sea conditions need to be modified accordingly. Meanwhile, although the modelling method of the flexible wire rope is similar as a whole, the actual modelling effect still has a close link with the knowledge of professionals, which may eventually lead to the differences in the mathematical model of the identified system. Overall, this work has presented an AHC method combining dynamics and intelligent control, providing new insights into the intelligence of marine hoisting equipment and into the development of equipment for marine mineral resources.

Code availability. To protect intellectual property rights and maintain the uniqueness of these academic achievements, the software code cannot be disclosed.

Data availability. The data can be obtained from https://pan.baidu.com/s/1f61dBmbpqgQH7SAzgoNTJg?pwd=9ymr (last access: 6 November 2026).

Author contributions. The authors confirm their contributions to the paper to be as follows: modelling and simulation, writing – TX; plan formulation – LH; proofreading – SW; experimental assistance – CZ. All of the authors reviewed and approved the final version of the paper.

Competing interests. The contact author has declared that none of the authors has any competing interests.

Disclaimer. Publisher's note: Copernicus Publications remains neutral with regard to jurisdictional claims made in the text, published maps, institutional affiliations, or any other geographical representation in this paper. The authors bear the ultimate responsibility for providing appropriate place names. Views expressed in the text are those of the authors and do not necessarily reflect the views of the publisher.

Acknowledgements. The authors gratefully acknowledge the financial support provided by the National Natural Science Foundation of China (grant no. 52075163).

Financial support. This research has been supported by the doctoral funding provided by the Hunan Institute of Engineering (grant no. 25RC013).

Review statement. This paper was edited by Liangliang Cheng and reviewed by four anonymous referees.

References

Calnan, C., Bauer, R. J., and Irani, R. A.: Reference-point algorithms for active motion compensation of towed bodies, IEEE J. Oceanic Eng.., 44, 1024–1040, https://doi.org/10.1109/JOE.2018.2866317, 2018.

Che, J. and Wang, S.: On the coupling mechanism of the large-amplitude swing motion in the floating crane vessel under wave action, Ocean Eng., 333, 121535, https://doi.org/10.1016/j.oceaneng.2025.121535, 2025.

Cuellar, W. H., Linhares, T. M., and Neto, A. B.: Passive and semi-active heave compensator: Project design methodology and control strategies, PloS one, 12, e0183140, https://doi.org/10.1371/journal.pone.0183140, 2017.

Guo, Y., Zhang, D., Chen, K., Feng, C., and Ge, S.: Longitudinal dynamic characteristics of steel wire rope in a friction hoisting system and its coupling effect with friction transmission, Tribol. Int., 119, 731–743, https://doi.org/10.1016/j.triboint.2017.12.014, 2018.

Huang, L., Zhang, Y., Sun, X., Jiang, H., Guo, X., and Zhang, W.: Design of hydraulic winch heave compensation system for offshore floating drilling, Acta Petrol. Sin., 38, 1091, https://doi.org/10.7623/syxb201709011, 2017.

Huang, Q., Li, Z., and Xue, H.: Multi-body dynamics co-simulation of hoisting wire rope, J. Strain Anal. Eng., 53, 36–45, https://doi.org/10.1177/0309324717744146, 2018.

Jin, R., Jiang, Y., Shen, W., Zhang, H., and Geng, B.: Coupled dynamic response of a tension leg platform system under waves and flow at different heading angles: An experimental study, Appl. Ocean Res., 115, 102848, https://doi.org/10.1016/j.apor.2021.102848, 2021.

Kim, H., Ranmuthugala, D., Leong, Z. Q., and Chin, C.: Six-DOF simulations of an underwater vehicle undergoing straight line and steady turning manoeuvres, Ocean Eng., 150, 102–112, https://doi.org/10.1016/j.oceaneng.2017.12.048, 2018.

Korde, U. A., Robinett III, R. D., and Wilson, D. G.: Wave-by-wave control in irregular waves for a wave energy converter with approximate parameters, Journal of Ocean Engineering and Marine Energy, 2, 501–519, https://doi.org/10.1007/s40722-016-0068-0, 2016.

Lawrence, C., Adytia, D., and Van Groesen, E.: Variational Boussinesq model for strongly nonlinear dispersive waves, Wave Motion, 76, 78–102, https://doi.org/10.1016/j.wavemoti.2017.10.009, 2018.

Li, S., Wei, J., Hu, B., and Li, S.: Nonlinear control of active heave compensator for an underwater towed system, J. Cent. South Univ. (Science and Technology), 49, 612–617, https://doi.org/10.11817/j.issn.1672-7207.2018.03.014, 2018.

Li, W., Wu, C., Lin, S., Li, G., and Zhang, P.: Active heave compensation of marine winch based on hybrid network prediction and sliding mode controller with a high-gain observer, Ocean Eng., 322, 120448, https://doi.org/10.1016/j.oceaneng.2025.120448, 2025.

Li, X., Mei, Z., Zhu, D., and Xie, B.: Modeling and anti-sway control of ship-mounted crane, Adv. Mech. Eng., 9, 1–9, https://doi.org/10.1177/1687814017727252, 2017.

Liao, W., Zhao, Y., Liu, D., and Jin, Y.: Active Heave Compensation Active Disturbance Rejection Control System of Electric Driven Marine Winches, China Mechanical Engineering, 29, 2999–3008, 2018.

Liu, M., Xu, B., and Peng, X.: Cooperative path planning for multi-AUV in time-varying ocean flows, J. Syst. Eng. Electron., 27, 612–618, https://doi.org/10.1109/JSEE.2016.00065, 2016.

Ma, C., Yao, J., Xiao, X., Di, X., and Jiang, Y.: Vibration Analysis of Winding Hoisting System based on ADAMS/Cable, The 3rd International Conference on Mechanical, Electrical and Material Application, Chongqing, China, 012033, https://doi.org/10.1088/1742-6596/1750/1/012033, 2021.

Nielsen, U. D., Brodtkorb, A. H., and Sørensen, A. J.: A brute-force spectral approach for wave estimation using measured vessel motions, Mar. Struct., 60, 101–121, https://doi.org/10.1016/j.marstruc.2018.03.011, 2018.

Richter, M., Schaut, S., Walser, D., Schneider, K., and Sawodny, O.: Experimental validation of an active heave compensation system: Estimation, prediction and control, Control Eng. Pract., 66, 1–12, https://doi.org/10.1016/j.conengprac.2017.06.005, 2017.

Schumacher, A., e Silva, S. R., and Soares, C. G.: Experimental and numerical study of a containership under parametric rolling conditions in waves, Ocean Eng., 124, 385–403, https://doi.org/10.1016/j.oceaneng.2016.07.034, 2016.

Tischler, M. B.: System identification methods for aircraft flight control development and validation, Advances in Aircraft Flight Control, 35–69, https://doi.org/10.1201/9781315136820-2, 2018.

Woodacre, J. K., Bauer, R. J., and Irani, R. A.: A review of vertical motion heave compensation systems, Ocean Eng., 104, 140–154, https://doi.org/10.1016/j.oceaneng.2015.05.004, 2015.

Woodacre, J. K., Bauer, R. J., and Irani, R. A.: Hydraulic valve-based active-heave compensation using a model-predictive controller with non-linear valve compensations, Ocean Eng., 152, 47–56, https://doi.org/10.1016/j.oceaneng.2018.01.030, 2018.

Xu, Z., Wang, Z., Shen, Z., and Sun, Y.: Nonlinear differential and integral sliding mode control for wave compensation system of ship-borne manipulator, Meas. Control, 54, 711–723, https://doi.org/10.1177/0020294020944956, 2021.

Zhang, W., Zou, Z., and Deng, D.: A study on prediction of ship maneuvering in regular waves, Ocean Eng., 137, 367–381, https://doi.org/10.1016/j.oceaneng.2017.03.046, 2017.

Zhang, Y., Shen, W., Long, Z., Zhang, Y., Wang, Z., Zhang Z., Zhu, S., Stocchino, A., Deng, H., and Zhu, H.: Active pendulation control of hoisting systems of ship-mounted cranes under ocean wave excitations: Principle and experimental study, Mech. Syst. Signal Pr., 222, 111802, https://doi.org/10.1016/j.ymssp.2024.111802, 2025.

Zhao, Y., Li, C., and Deng, Y.: Modeling and simulation analysis on the control system of marine shipborne electric driven winch, Computer Simulation, 33, 244–249, 2016.

Zhou, B., Hu, Y., and Zhu, H.: Dynamic simulation and experimental investigation of the double-rope winding hoister based on an equivalent mechanical model of wire ropes, Structures, 69, 107237, https://doi.org/10.1016/j.istruc.2024.107237, 2024.